

# SCANNING BEAM RADAR ALTIMETRY FOR LAND SURFACE MONITORING

Sune R. J. Axelsson

Microwave Systems  
Saab Missiles AB  
S-581 83 Linköping  
Sweden  
Commission I

## ABSTRACT

The Skylab experiment followed by GEOS-3, Seasat and Geosat clearly showed the capability of spaceborne radar altimetry for oceanographic applications such as measurements of wave-height, tidal action and the deviation from the perfect geoid. Over land areas, however, their use is highly restricted due to the limited ground resolution, the sensitivity to off-track topography and local variations in surface reflectivity. For that reason, future radar altimeters more specifically designed for land surface monitoring should use narrow-beam antennas with across-scanning capability. In this paper, the performance of such an instrument is analyzed in detail. Three types of imagery can be generated by the sensor: (i) surface topography, (ii) characteristic subpixel roughness height, and (iii) the radar reflectivity of ground at near-nadir angles of observation. Main characteristics of the altimetry data over various types of land surfaces are discussed.

## 1 INTRODUCTION

The first generation of spaceborne radar altimeters, such as Skylab (1973), GEOS-3 (1975), Seasat (1978) and Geosat (1985) have clearly proved the capability of the technique for measurements of wave height, tidal action, and the deviation from the perfect geoid [1] - [5]. Similar kinds of instruments but with improved performance will be carried by ERS-1 and the Topex satellite [6], [7].

All these altimeters were mainly designed for oceanographic applications. They use a fixed nadir-oriented antenna with a foot-print diameter of about 20 km. Frequency-modulated pulses are transmitted towards the sea-surface, and in the receiver, the return waveform is detected after pulse compression in an array of range cells. The altitude is then estimated from the delay of the leading edge of the pulse return. The slope of the leading edge is a measure of the significant wave height.

The range resolution of the above altimeters was gradually improved from about 20 m for Skylab, 2 m for GEOS-3 and 0.5 m for Seasat, which gives a precision at altitude measurements over oceans from 1 m for Skylab to about 5 cm precision for Seasat.

For a near-flat surface like the sea, the leading edge of the pulse response is generated by reflectors located in an area close to the nadir direction. The plateau and back of the return are built up by responses from more slanting directions.

When the surface roughness increases, the reflector range in the nadir direction becomes more varying. As a result, the slope of the leading edge is reduced and the contributing area is widened.

Consequently, the foot-print area of the leading edge highly depends upon the surface topography. Over a sea-surface with a wave height of 4 m, for instance, the foot-print radius of the leading edge is about 2 km (ERS-1) but can increase to 8 km over a rough land area.

Therefore, pulse-limited radar altimeters are mainly useful for large-scale profiling and at estimations of the characteristic surface roughness height of near-flat surfaces like the ocean. Over land areas the ground resolution becomes too poor for most applications, however. Contrary to oceanographic profiling, the leading edge of the return pulse is more affected by off-track topography and strong local variations in surface reflectivity.

Consequently, the ground resolution of future altimetry systems more specifically dedicated to ice- and land-surface mapping, should be radically improved. The ultimate aim would be a spatial resolution of about 200x200 m and an error at the altitude estimation of less than one metre. In order to achieve annual mapping of the globe, the swath-width should exceed 6 km.

In this paper, the design and performance of such an Advanced Scanning Radar Altimeter (ASRA) will be further discussed.

## 2 NARROW-BEAM IMAGING RADAR ALTIMETRY

### 2.1 Principles of operation

The above requirements on mapping capability might be satisfied by using a more advanced radar altimeter with a very narrow antenna beam, which is scanned across the satellite track.

Besides improved topographic and local surface roughness information, this sensor also provides high-resolution maps of the surface reflectivity close to the nadir direction, which often contains a significant amount of near-specular returns. The imagery will be a useful complement to conventional SAR-data from more oblique angles of observation.

By introducing multiple doppler beams in the forward direction, each resolution cell can be observed at several different angles of incidence as well.

The pulse response of the surface is detected in  $N$  range cells representing the ranges  $R_0 + k\Delta R$  (where  $k = 0$  to  $N$ ) in a similar way as for the first generation of altimeters. Parallel range arrays for each dopplerbeam may be necessary, however, for onboard signal processing.

From the range cell samples ( $A_k, R_k$ ), the mean range to the resolution element can be estimated using

$$\tilde{R} = \frac{1}{A_0} \sum_{k=1}^N A_k R_k \quad (2.1)$$

where

$$A_0 = \sum_{k=1}^N A_k \quad (2.2)$$

is for a square-law envelope detector a direct measure of the reflectance of the resolution element.

From the radar equation and the beam geometry,  $A_0$  is easily translated into the back-scattering coefficient of the resolution element ( $\sigma^0$ ).

For estimations of the local surface roughness height in the resolution cell, the range spread (rms)  $\sigma_R$  is also of interest defined by

$$\sigma_R^2 = \frac{1}{A_0} \sum_{k=1}^N A_k (R_k - \tilde{R})^2 \quad (2.3)$$

The third and fourth orders of central moments

$$m_n = \frac{1}{A_0} \sum_{k=1}^N A_k (R_k - \tilde{R})^n \quad (2.4)$$

might also be used to further specify the characteristics of the pulse shape, such as the skewness and the excess.

For more detailed analyses of the pulse shape, the full information content of the range cells  $\{A_k, R_k\}$  might be necessary.

## 2.2 Antenna size

The requirement of a ground resolution of the order of 200 m calls for very large antenna dimensions across-track. In the forward direction, the extent can be reduced, however, because narrow beams are easily generated using dopplerbeam sharpening or synthetic aperture technique.

At the carrier frequency 35 GHz and the orbit altitude 800 km, an antenna length of 40 m is required across-track in order to achieve a ground resolution of 200 m. For an altimeter carried by the space shuttle ( $H = 240$  km), the across track dimension would be reduced to 12 m, however.

Further size reductions are possible in the 95 GHz-band, giving  $L = 15$  m ( $H = 800$  km) and 4.5 m ( $H = 240$  km), respectively. A disadvantage is the increased atmospheric influence at higher frequencies, which will make it necessary to correct for the atmospheric effect upon the pulse-delay.

### 2.3 Imaging performance

By electronic scanning of the antenna beam across track, an imaging mode is introduced. For each position of the beam, a number of resolution elements can be measured simultaneously along-track using parallel doppler-filter processing.

The doppler bandwidth corresponding to the extension of the resolution element along-track ( $d$ ) is given by:

$$B_d = \frac{2v}{\lambda} \frac{d}{H} \quad (2.5)$$

for near-nadir observations.

The minimum time of observation is:

$$\tau \approx \frac{1}{B_d} = \frac{\lambda H}{2dv} \quad (2.6)$$

In order to get continuous mapping, the time per each scan should not exceed:

$$\tau_s = dN/v \quad (2.7)$$

where  $N$  is the number of simultaneous doppler beams in the along-track direction. The swath-width is then limited by:

$$w = \frac{\tau_s}{\tau} d = \frac{2d^3 N}{\lambda H} \quad (2.8)$$

Example: For  $d = 200$  m,  $\lambda = 0.01$  m,  $H = 800$  km, a maximum swath-width of 2 km is obtained for single beam scanning ( $N = 1$ ). With parallel doppler filter processing and  $N = 10$ , a swath-width of 20 km might be covered. An increase of  $N$  to 100 and unchanged swath-width makes multiple looks possible (10 looks with 2 km separation).

If  $H = 240$  km, the single-beam swath-width ( $N = 1$ ) is increased to about 7 km. For  $N = 30$  and a swath-width of 20 km, it would be possible to observe each surface element 10 times with a separation of 600 m.

To make it possible to extract the doppler frequency, the pulse frequency should be at least twice as high as the maximum doppler-frequency of the return signal i.e.

$$f_r > 2NB_d$$

If  $d = 200$  m,  $\lambda = 0.01$  m,  $H = 800$  km and  $v \approx 8000$  m/s as in the example above, we find  $B_d = 400$  Hz from (2.5). Hence, a repetition frequency of the order of 10 kHz or more is required for  $N = 10$ .

In order to restrict the total doppler bandwidth of the return signal to  $N \cdot B_d$  the along track beam width of the antenna should be  $\theta_A \approx 2Nd/H_0$ , i.e. 5 mrad in the last example.

### 3 SIMULATION MODEL

#### 3.1 General

The characteristics of the pulse return from an arbitrary ground surface can be predicted by computer simulations as described in [8].

The foot-print area of the antenna and its first side-lobes are then covered by a grid  $(n,m)$  of resolution  $\Delta d$  and  $-N \leq n < N$ ,  $-M \leq m \leq M$ . For each square of the grid, the radar cross-section per unit area of the ground  $\sigma^o(n,m)$  and the height deviation  $h(n,m)$  from a reference surface are defined. The reflectivity is represented by a point reflector located at range  $R(n,m)$  with the radar cross-section  $\sigma = (\Delta d)^2 \sigma^o(n,m)$ .

The x-, y-coordinates of the reflectors in a coordinate system with its origin in the subsatellite point are

$$\begin{aligned} X_n &= X_S + (n+0.5)\Delta d \\ Y_n &= Y_S + (m+0.5)\Delta d \end{aligned} \quad (3.1)$$

where  $X_S, Y_S$  represents the centre of the antenna foot-print area.

The received power from each resolution element  $(n,m)$  is estimated from the radar equation:

$$P(n,m) = \frac{P_S \lambda^2 G^2(n,m) \sigma^o(n,m) (\Delta d)^2}{(4\pi)^3 L_p R^4(n,m)} \quad (3.2)$$

where  $P_S$  is transmitted power,  $\lambda$  is the electromagnetic wavelength,  $L_p$  represents atmospheric attenuation and system losses in the receiver, and  $G(n,m)$  is the antenna gain in the direction of the resolution element  $(n,m)$ .

If  $H_0$  represents the altitude of the satellite above a reference surface, the distance to the reflecting point of element  $(n,m)$  is given by (Fig 1):

$$R(n,m) = [(H_0 + R_0)^2 + (R_0 + h)^2 - 2(H_0 + R_0)(R_0 + h)\cos\phi]^{1/2} \quad (3.3)$$

where

$$\begin{aligned} \phi(n,m) &= r(n,m)/R_0 \\ r(n,m) &= (X_n^2 + Y_m^2)^{1/2} \end{aligned} \quad (3.4)$$

and  $R_0$  is the local radius of a spherical reference surface approximation.

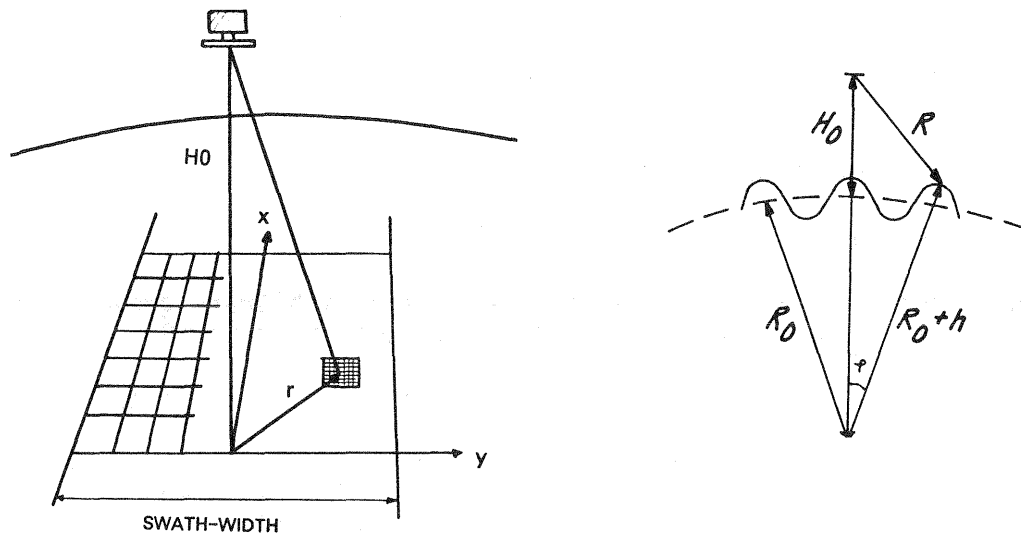


Figure 1. Definition of geometry.

By using the fact that  $h \ll R_0$  and  $\phi \ll 1$ , the following approximation of (3.3) can be applied:

$$R(n,m) = H_0 - h(n,m) + (X_n^2 + Y_m^2) / (2H_e) \quad (3.5)$$

in which:

$$\frac{1}{H_e} = \frac{1}{R_0} + \frac{1}{H_0}. \quad (3.6)$$

The broadening effect of the pulse width can be taken into account by a convolution of the impulse function return from the ground with:

$$p(x) = \frac{1}{\sqrt{2\pi}\sigma} \exp\left(-\frac{x^2}{2\sigma^2}\right) \quad (3.7)$$

where

$$\sigma = \frac{c}{2} \tau_p \quad (3.8)$$

and  $\tau_p$  represents the root-mean-square width of the transmitted pulse.

An alternative more simplified method is to add a Gaussian range noise component to eqn. (3.3) or (3.5) with zero mean and variance according to eqn. (3.8).

### 3.2 Single-pulse response

Equations (3.1) - (3.6) define the range and power received from a reflector located at  $(X_n, Y_m)$  and  $h(n,m)$  above the reference surface. Each range bin of the receiver defines a range interval  $R_K \pm \Delta R_b$ , where  $\Delta R_b$  is half the range resolution.

Let us now subdivide the grid into subsets  $S_K$  with  $K = 1$  to  $N_b$  corresponding to the different range bins in such a way that  $S_K$  will represent all reflectors  $(n,m)$  on ground satisfying  $R_K - \Delta R_b < R(n,m) < R_K + \Delta R_b$ . Hence:

$$S_K = \{(n,m) \mid \text{Abs}(R_K - R(n,m)) < \Delta R_b\} \quad (3.9)$$

The amplitude of the pulse return in the  $K$ -th range bin is then estimated from:

$$A_K = (U_K^2 + V_K^2)^{1/2} \quad (3.10)$$

where

$$\begin{aligned} U_K &= \sum_{S_K} \sqrt{2P(n,m)} \cos[\alpha(n,m)] \\ V_K &= \sum_{S_K} \sqrt{2P(n,m)} \sin[\alpha(n,m)] \end{aligned} \quad (3.11)$$

and

$$\alpha(n,m) = \frac{4\pi}{\lambda} R(n,m) + \beta(n,m) \quad (3.12)$$

Over a rough, incoherently scattering surface,  $\alpha(n,m)$  is uniformly distributed  $(0, 2\pi)$ . If no reflector gives a dominating response,  $U_K$  and  $V_K$  are Gaussian and statistically independent with zero means. As a result,  $A_K$  becomes Rayleigh-distributed with the probability density function:

$$p(A_K) = \frac{A_K}{P_K} \exp\left(-\frac{A_K^2}{2P_K}\right) \quad (3.13)$$

where  $P_K$  is the total received power in the  $K$ -th range bin:

$$P_K = \sum_{S_K} P(n,m) \quad (3.14)$$

The relationships (3.10) and (3.13) presume a linear envelope detector. For a square-law detector, the envelope of the pulse return is given by  $B_K = U_K^2 + V_K^2$  and eqn. (3.13) is replaced by an exponential distribution.

### 3.3 Mean pulse response

As a result of the pulse-to-pulse variations of  $\alpha(n,m)$  in eqn. (3.11) the envelope samples  $A_K$  are fading. The mean pulse response is obtained by averaging eqn. (3.10) with  $\alpha$  uniformly distributed  $(0,2\pi)$ . For a non-specular surface with Rayleigh-distributed envelope (linear detector):

$$\overline{A_K} = \sqrt{\frac{\pi}{2} P_K} \quad (3.15)$$

For a square-law detector, the average output is  $2P_K$ .

### 3.4 Smoothed pulse response

Usually, the single-pulse response alone is not very useful at the data analysis due to fading effects. Instead, the average of a great number ( $N_p$ ) of pulse responses is formed:

$$A_{SK} = \frac{1}{N_p} \sum_{n=1}^{N_p} A_{Kn} \quad (3.16)$$

where  $A_{Kn}$  is the envelope of the  $n$ -th pulse return in the  $K$ -th range bin.

In a general simulation model, the range variation effect is taken into account by computing the individual single-pulse responses, which are fed into the subsequent averaging and tracking algorithms. A disadvantage of this method, however, is the long computer time required. More rapid approximative methods were discussed in [8].

Over surfaces with a low amount of coherent scattering, the correlation between neighbouring pulses can usually be neglected, if pulse-limited altimeters, such as Seasat or ERS-1, are used. For a beam-limited altimeter with  $d = 200$  m,  $H = 800$  km,  $\lambda = 0.01$  m and  $v = 8000$  m/s, the doppler bandwidth is only 400 Hz, which means a high correlation between adjacent pulses for pulse repetition frequencies exceeding 1000 Hz.

## 4 ACCURACY

### 4.1 General

From Eqs. (2.2) and (2.3), the centroid of the return pulse indicates the average range to the reflectors inside the resolution cell, while the pulse width is a measure of the range spread or the local surface roughness.

From (2.2), it is obvious, however, that a true mean range is generally not obtained at radar altimetry. Due to fading effects and sub-pixel variations in surface reflectivity, the centroid of a single pulse return represents more correctly a weighted average range. Also the rms width of the pulse return according to (2.3) means a weighted range spread.

Over homogeneous surfaces, the statistics of the fading envelope according to (3.13) - (3.14) gives a main contribution to the estimation errors of mean range and rms range spread. The influence of fading is minimized by smoothing several statistically independent pulse envelopes. A smoothing effect at the estimation of  $R$  and  $\sigma_R$  is also obtained, when the range spread ( $\sigma_R$ ) is much larger than the range resolution ( $\Delta R$ ) of the altimeter.

## 4.2 Inhomogeneous resolution cells

For inhomogeneous surfaces, variations in surface reflectance can give significant errors. Let us as an example consider the case, when the pulse response originates from two surfaces with different reflectance ( $\sigma_1^0$  and  $\sigma_2^0$ ) and located at the distances  $R_1$  and  $R_2 = R_1 + D$ , respectively, from the altimeter. If the two surfaces cover the portions  $p_1$  and  $p_2 = (1 - p_1)$  of the foot-print area, the true average range ( $R$ ) and rms range spread ( $\sigma$ ) are

$$\begin{aligned}\bar{R} &= p_1 R_1 + p_2 R_2 = R_1 + (1 - p_1) D \\ \sigma &= \sqrt{(R - \bar{R})^2} = \sqrt{p_1 (1 - p_1)} D\end{aligned}\quad (4.1)$$

If we neglect the fading effect, the weighted average range and rms value measured by the altimeter are given by a formally similar expression

$$\begin{aligned}\tilde{R} &= R_1 + (1 - p) D \\ \sigma_R &= \sqrt{p(1 - p)} D\end{aligned}\quad (4.2)$$

but with the weighting factor redefined as

$$p = \sigma_1^0 p_1 / (\sigma_1^0 p_1 + (1 - p_1) \sigma_2^0)\quad (4.3)$$

Hence, (4.1) and (4.2) agree, only if  $\sigma_1^0 = \sigma_2^0$ . The relationships (4.2)-(4.3) also mean that ground surface elements with strong reflectance are given an increased importance at the averaging procedure.

If  $p = 0.5$  and  $\sigma_1^0 = 0.1 \sigma_2^0$ , for instance,  $\bar{R} = R_1 + 0.5D$  and  $\sigma = 0.5D$ , while

$$\begin{aligned}\tilde{R} &= R_1 + 0.9D \\ \sigma_R &= 0.3D\end{aligned}$$

are predicted from the received pulse waveform.

Consequently, significant errors are generated, when the altimeter beam crosses the boundary between two different kinds of surfaces. An extreme case is when the altimeter beam passes from sea in over an elevated land plateau. Due to the much higher back-scattering from the water, the altimeter measures the range to the water surface until almost the complete sensitivity beam is taken up by land surface reflectors. As a result the detected shore-line profile is displaced half a resolution element.

Similar types of errors are obtained over volume scattering mediums such as forests. The detected centroid range ( $\tilde{R}$ ) and range spread ( $\sigma_R$ ) are then highly influenced by the scattering characteristics of the ground surface and the tree elements. Some a priori knowledge of the scattering behaviour will improve the accuracy at estimations of significant tree height or tree density, based upon  $\sigma_p$  or a more detailed pulse shape analysis. Predicted pulse responses from forests are shown in Figure 3 assuming homogeneous reflectance.

### 4.3 Sloping effects

In general, the accuracy of the altimetry measurements will be reduced, if the surface element is not perpendicular to the sensitivity beam. This means that some degradation is obtained for sloping surface elements, or resolution cells which are far away from the subsatellite point.

Let us analyse this behaviour for homogeneous surface elements. If fading effects are neglected, we can approximately express the normalized beam function as follows:

$$g(x,y) = \frac{1}{2\pi\sigma_x\sigma_y} \exp\left[-\frac{(x-x_0)^2}{2\sigma_x^2} - \frac{(y-y_0)^2}{2\sigma_y^2}\right]$$

where  $x = y = 0$  is the subsatellite point,  $(x_0, y_0)$  defines the centre of the resolution element on ground, and  $\sigma_x, \sigma_y$  are the rms widths of the resolution element along-track and across-track, respectively.

According to Eqs. (3.5), the range to a reflector on the ground located  $h(x,y)$  above a spherical reference surface can be described by

$$R(x,y) = H_0 - h(x,y) + (x^2 + y^2)/2H_e \quad (4.4)$$

Let us describe the local variations of  $h(x,y)$  within the surface element at  $(x_0, y_0)$  as

$$h(x,y) = h_0 + a(x-x_0) + b(y-y_0) + \eta(x,y) \quad (4.5)$$

where  $h_0$  is the weighted mean deviation from the reference surface, and  $a, b$  are the local mean surface slopes in  $x$ - and  $y$ -directions. The deviation between the real surface topography and the sloping plane surface approximation is defined by  $\eta(x,y)$ .

The first and second moments of the impulse response from the antenna foot-print area can be derived from:

$$\begin{aligned} \tilde{R} &= \iint g(x,y)R(x,y)dx dy \\ \tilde{R}^2 &= \iint g(x,y)R^2(x,y)dx dy \end{aligned} \quad (4.6)$$

where  $\tilde{R}$  corresponds to the centroid of the pulse return.

The rms width of the return pulse is thus:

$$\sigma = \sqrt{\tilde{R}^2 - (\tilde{R})^2} \quad (4.7)$$

Substitution of (4.4) - (4.5) into (4.6) yields after simplifications

$$\tilde{R} = H_0 - h_0 + (x_0^2 + y_0^2 + \sigma_x^2 + \sigma_y^2) / 2H_e \quad (4.8)$$

The equation means that the measured elevation ( $h$ ) of a resolution cell at  $(x_0, y_0)$  has a negative bias error given by

$$\Delta h = (x_0^2 + y_0^2 + \sigma_x^2 + \sigma_y^2) / 2H_e \quad (4.9)$$

As an example, a bias of 0.6 m is obtained for  $H_e = 800$  km,  $x_0 = 0$  and  $y_0 = 1$  km. For  $y_0 = 4$  km,  $\Delta h$  is increased to 10 m. This error can be corrected, however, since  $x_0$ ,  $y_0$ ,  $\sigma_x$  and  $\sigma_y$  are supposed to be known.

From (4.9), an uncertainty in  $x_0$ ,  $y_0$  will give the following error after bias correction

$$\Delta h_c = (x_0 \cdot \Delta x_0 + y_0 \cdot \Delta y_0) / H_e \quad (4.10)$$

For  $H_e = 800$  km,  $x_0 = 0$ ,  $y_0 = 4$  km and  $\Delta y_0 = 100$  m, an elevation error of  $\Delta h = 0.5$  m is obtained. For a swath width of 20 km ( $y_0^{\text{Max}} = 10$  km) the error is increased to 1.2 m. At low orbit measurements from the space shuttle (240 km), the bias is increased a 3.3 factor.

Sloping terrain and off-nadir observations have also a significant effect upon the detected pulse width. From (4.4) - (4.8), the rms range spread ( $\sigma_R$ ) is given by

$$\sigma_R^2 = \sigma_\eta^2 + \sigma_x^2 (a - x_0 / H_e)^2 + \sigma_y^2 (b - y_0 / H_e)^2 \quad (4.11)$$

where

$$\sigma_\eta^2 = \tilde{\eta}^2 - \eta^2 \quad (4.12)$$

is the local surface roughness height (rms) that would be measured at nadir observations over a horizontal surface ( $a = b = x_0 = y_0 = 0$ ).

From (4.11), we find for  $H_0 = 800$  km and  $\sigma_x = \sigma_y = 100$  m (i.e. a resolution element of 200 x 200 m) that a flat horizontal surface element gives  $\sigma_R = 1.2$  m, when the sensitivity is pointing 10 km off-track.

If  $H_0 = 240$  km,  $\sigma_R$  is increased to 4 m.

For non-horizontal surface elements, the pulse response is further widened. If  $a = 0$  and  $b = 0.03$  (i.e. two degrees inclination),  $\sigma_R = 3$  m is obtained for  $H_0 = 800$  km and resolution elements close to the subsatellite point ( $x_0 = y_0 = 0$ ).

Even in that case, however, the increased roughness response from groups of trees should be detectable using the  $\sigma_R$ -value.

If the topographic variations have a correlation length larger than the resolution element, most of the sloping effect can be compensated by using  $\tilde{R}$ -estimates of adjacent resolution cells.

Over flat areas such as a water surface or sea-ice, the sloping surface effects can usually be neglected ( $a = b = 0$ ). The range spread variation with scanning angle  $(x_0, y_0)$  in (4.11) can then be compensated for, which improves the sensitivity at monitoring areas with ice-ridges, for instance. Examples of predicted pulse responses from sea-ice are shown in Figure 4.

## 5 CONCLUSIONS

The design and performance of an Advanced Scanning Radar Altimeter (ASRA) for high-resolution topographic mapping have been analysed and discussed. This type of sensor also provides information about the significant surface roughness height and back-scattering coefficient of each resolution cell.

A difficult point at the implementation of such an instrument is the large antenna aperture required to get a sufficiently narrow beam. By using a higher carrier frequency (35 or 95 GHz) than in earlier altimetry applications and doppler beam sharpening technique in the along-track direction, the antenna can be reduced to a more convenient size.

The analysis also shows upon a growing altitude bias, when the off-nadir angle is increased. This effect restricts the usable swath-width at high-precision profiling.

The accuracy of surface roughness height estimations based upon the pulse width will also be significantly reduced over hilly ground and over non-homogeneous areas with great backscattering variations.

## ACKNOWLEDGEMENTS

Parts of this research were carried out at Linköping University with financial support from the Swedish Board for Space Activities. I am also grateful to Ing-Marie Pilemalm for typing this manuscript.

## REFERENCES

- [1] Dooley, R.P. and Brooks, L.W., 1974. Radar altimetry and ocean wave height estimation. Technology Service Corporation, Maryland, Contract NAS6-2241.
- [2] McGoogan, J.T., Miller, L.S., Brown, G.S. and Hayne, G.S., 1974. The S-193 Radar altimeter experiment. Proc. IEEE, 62 (6): 793-803.
- [3] Townsend, W.F., 1980. An initial assessment of the performance achieved by the Seasat-1 Radar Altimeter, IEEE J. Oceanic Engin., vol. OE-5:2, pp 80-92.

- [4] Born, G.H., Lame, D.B., Mitchell, M.D., 1984. A survey of oceanographic satellite altimetric missions. J.Mar. Geod., vol. 8, pp 3-16.
- [5] The Navy GEOSAT Mission. Johns Hopkins APL Technical Digest, vol. 8, No. 2, 1987.
- [6] Rapley, C.G. et al., 1985. Applications and scientific uses of ERS-1 radar altimeter data. ESA report 5684/83/NL/BI.
- [7] Born, G.H., Stewart, R.H., Yamarone, C.A., 1985. Topex - A spaceborne ocean observing system. From Monitoring Earth's Ocean, Land and Atmosphere from Space-Sensors, Systems and Applications, edited by A.Schnapf, vol. 97 of Progress in Astronautics and Aeronautics series, pp. 464-479.
- [8] Axelsson, R.S.J., 1987. Radar altimetry response from rough surfaces. Photogrammetria, vol. 42, pp. 1-18.

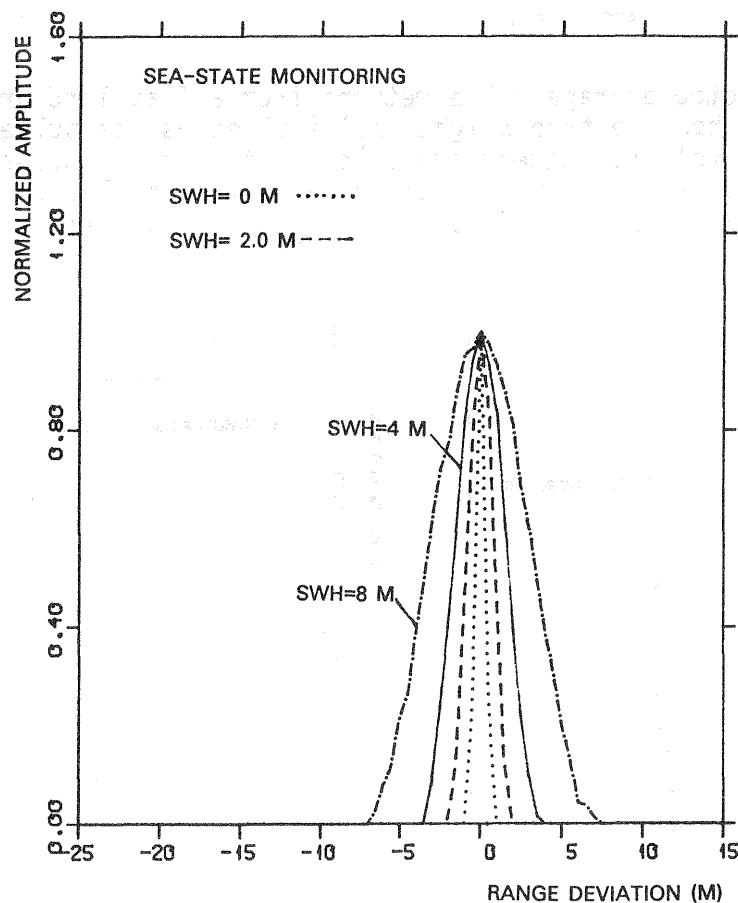


**Figure 2.** Predicted average pulse responses from a sea-surface versus significant wave height for  $\sigma_x = \sigma_y = 100$  m,  $H_0 = 800$  km,  $x_0 = y_0 = 0$ ,  $\Delta R = 0.5$  m (linear detector).

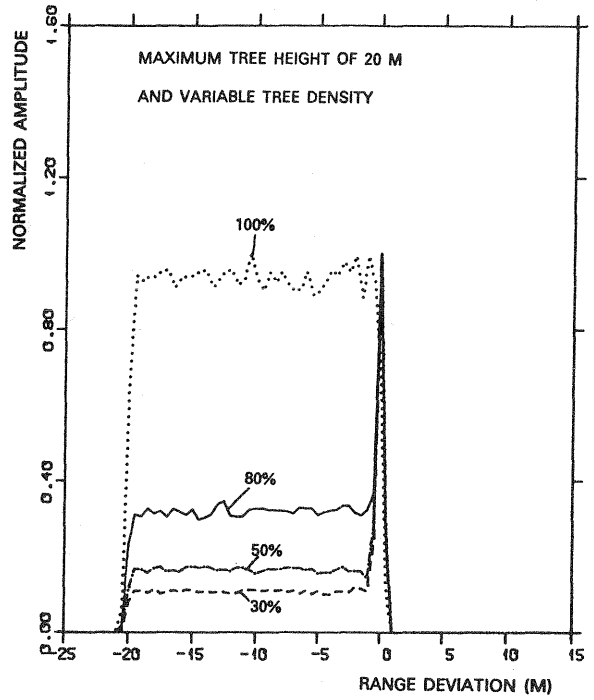
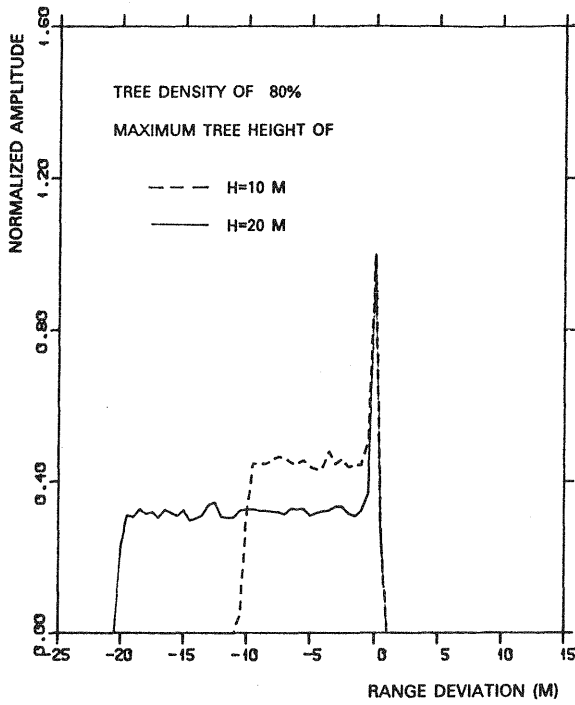


Figure 3. Predicted average pulse returns from a flat land area covered by wood, showing how the tree height ( $h_0$ ) influences the pulse-width and the tree density ( $p$ ) the plateau amplitude of the tree response. Homogeneous reflectance, uniformly distributed tree reflectors with height  $(0, h_0)$ ,  $\Delta R = 0.5$  m,  $\sigma_x = \sigma_y = 100$  m, and  $x_0 = y_0 = 0$  were assumed.

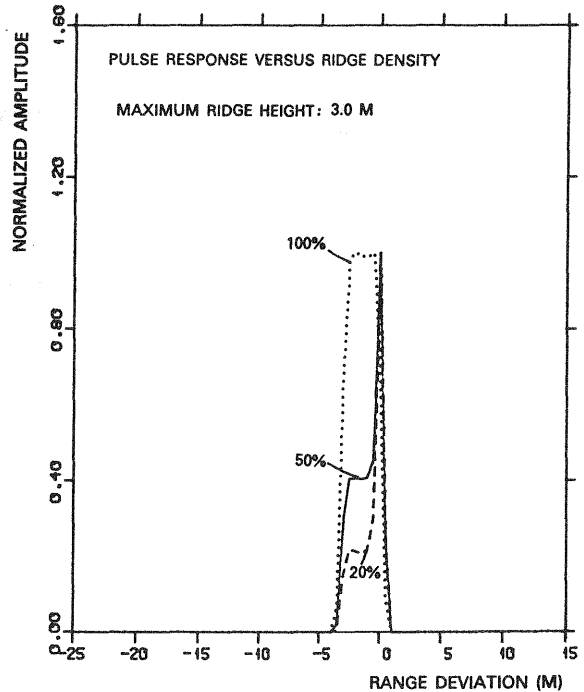
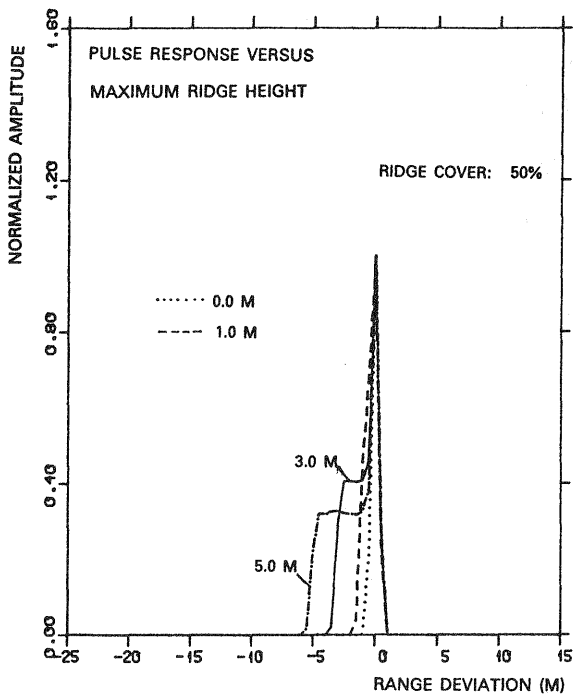


Figure 4. Predicted average pulse returns from rough sea-ice with ridges showing the influence of height and density upon the pulse shape.